

Passive Thermal Control for the Low Density Supersonic Decelerator (LSD) Test Vehicle Spin Motors Sub-System

Matthew Redmond¹, A.J. Mastropietro², and Michael Pauken³
NASA Jet Propulsion Laboratory, California Institute of Technology, Pasadena, California, 91109

and

Brandon Mobley⁴
NASA Marshall Space Flight Center, Huntsville, Alabama, 35812

Future missions to Mars will require improved entry, descent, and landing (EDL) technology over the Viking-heritage systems which recently landed the largest payload to date, the 900 kg Mars Science Laboratory. As a result, NASA's Low Density Supersonic Decelerator (LSD) project is working to advance the state of the art in Mars EDL systems by developing and testing three key technologies which will enable heavier payloads and higher altitude landing sites on the red planet. These technologies consist of a large 33.5 m diameter Supersonic Disk Sail (SSDS) parachute and two different Supersonic Inflatable Aerodynamic Decelerator (SIAD) devices – a robotic class that inflates to a 6 m diameter torus (SIAD-R), and an exploration class that inflates to an 8 m diameter isotenoid (SIAD-E). All three technologies will be demonstrated on test vehicles at high earth altitudes in order to simulate the Mars EDL environment. Each vehicle will be carried to altitude by a large helium balloon, released, spun up using spin motors to stabilize the vehicle's trajectory, and accelerated to supersonic speeds using a large solid rocket motor. The vehicle will then be spun down using another set of spin motors, and will deploy either the SIAD-R or SIAD-E, followed by the SSDS parachute until the vehicle lands in the ocean. Component level testing and bounding analysis are used to ensure the survival of system components in extreme thermal environments and predict temperatures throughout the flight. This paper presents a general description of the thermal testing, model correlation, and analysis of the spin motor passive thermal control sub-system to maintain spin motor performance, prescribed vehicle trajectory, and structural integrity of the test vehicle. The spin motor sub-system is predicted to meet its requirements with margin.

Nomenclature

c_p	= Specific heat	CEC	= Chemical Equilibrium Combustion
k	= Thermal conductivity	CFD	= Computational Fluid Dynamics
q''	= Heat flux	EDL	= Entry, Descent, and Landing
T	= Temperature	LSD	= Low Density Supersonic Decelerator
t	= Time	$PLIMP$	= Plume Impingement code
ε	= Thermal emissivity	$RAMP2$	= Reacting and Multiphase Program, version 2
π	= Pi	$SIAD$	= Supersonic Inflatable Aerodynamic Decelerator
ρ	= Density	$SSDS$	= SuperSonic Disk Sail
σ	= Stefan-Boltzman constant	TPS	= Thermal Protection System
AFT	= Allowable Flight Temperature	WCC	= Worst Case Cold
$BLDT$	= Balloon Launched Decelerator Test	WCH	= Worst Case Hot

¹ Thermal Systems Engineer, Thermal and Fluids System Engineering Group.

² Thermal Systems Engineer, Thermal and Fluids System Engineering Group.

³ Senior Thermal Systems Engineer, Thermal and Fluids System Engineering Group.

⁴ Aerothermodynamics Engineer, EV33/Aerosciences Branch.

I. Introduction

Previous lander missions to Mars have all relied on heritage landing technology developed for the Viking program in the 1970s and tested on balloon launched decelerator test vehicles (BLDT)¹⁻³. However, future missions to Mars will require new types of decelerator systems in order to land heavier payloads at higher altitudes. Although many different types of decelerator systems have been studied over the past 50 years⁴ NASA's Low Density Supersonic Decelerator (LSD) program has been tasked with developing and testing three new decelerator technologies to enable future missions, shown in Figure 1. One of these, the Supersonic Disk Sail (SSDS) parachute is similar to the Disk-Gap-Band parachute tested during the BLDT program. The other two are Supersonic Inflatable Aerodynamic Decelerator (SIAD) devices. The SIAD-R is a 6 meter outside diameter torus intended for robotic missions which inflates using compressed gas. The SIAD-E is an 8 meter outside diameter isotoisoid intended for human exploration missions which inflates using a combination of compressed gas and ram air. Details on the development of the parachute, SIADs, test vehicle can be found in⁵⁻⁷.

All three technologies are planned for testing at the Pacific Missile Range Facility on Kauai, Hawaii during the summers of 2014 and 2015⁹. The flight profile of the vehicle is summarized in Figure 2. The test vehicle is launched using a helium filled balloon provided by Columbia Scientific Balloon Facility. When it reaches a float altitude of approximately 118,000 ft (~36 km), the test vehicle is dropped, spun up for trajectory stability using solid propellant spin up motors, and a large solid rocket motor fires to accelerate the test vehicle to around Mach 4. Once the main motor burn is finished, the vehicle is de-spun using a set of spin down motors and the test period begins. The SIAD is tested first, followed by a test of the SSDS parachute, and concluding with a descent into the ocean and subsequent recovery. The flight spans a number of environmental regimes including ascent, float, test, and descent which can be thermally challenging. In particular, the long ascent and float through the cold air in the upper atmosphere and the large heat fluxes encountered during the solid rocket burns have proved challenging to manage in both the LSD test vehicle and the previous Viking-era BLDT test^{10,11}.

The focus of this work is the LSD test vehicle spin motor sub-system. First, an overview is given of the spin motor sub-system and the sub-system requirements are discussed. Next, a spin motor thermal model is presented along with its calibration to ground test firing data. The predicted spin motor plume heating and TPS temperature predictions are also discussed. Finally, the predicted temperatures of the spin motors prior to firing are presented, and top deck heating due to soakback is analyzed. The spin motors, top deck, and TPS system are all predicted to meet their requirements with margin.

II. Spin Motor Sub-System Overview

A total of eight spin motors, four spin up and four spin down, are located on the exterior of the test vehicle as shown in Figure 3. The spin up motors are numbered 1-4 (red) and the spin down motors are numbered 5-8 (green).

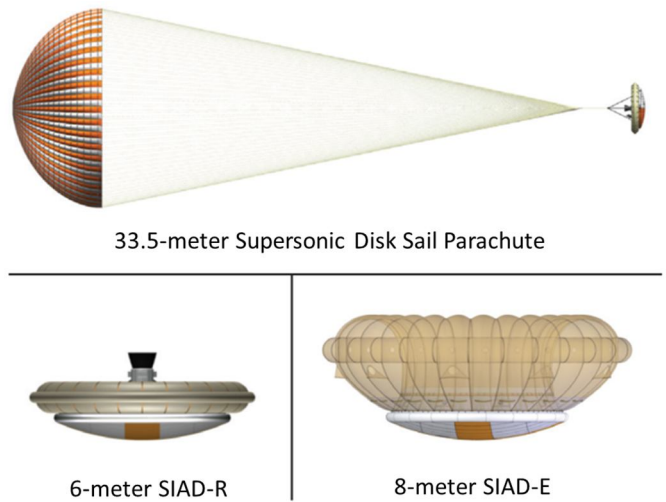


Figure 1. Parachutes tested in the LSD test program⁸.

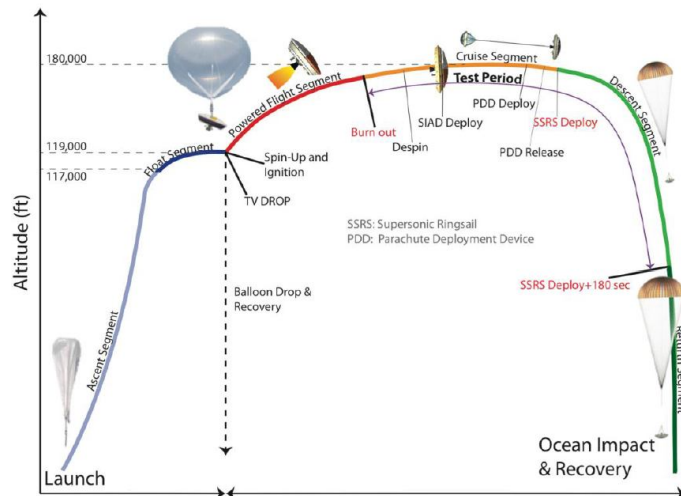


Figure 2. Summary of the flight profile⁹.

Multiple spin motor firing configurations have been considered through the course of the project. In the simultaneous firing scenario, all four spin up motors fire concurrently, followed by the main motor burn, followed by all four spin down motors firing concurrently. For the staggered firing scenario, there are a total of four spin motor pairs which fire in sequence before and after the main motor burn. The sequence of motor burns in the staggered firing scenario is as follows: spin motors 1 and 3, spin motors 2 and 4, main motor, spin motors 6 and 8, and then spin motors 5 and 7. It is necessary for the spin motors to fire in pairs to apply a moment couple to the vehicle without generating excessive nutation. In addition, the amount of force generated by the spin motors is dependent on the initial propellant temperature, so large differences in spin motor temperature could affect the vehicle trajectory and stability.

The primary thermal focus is on predicting spin motor temperatures prior to spin motor firing and mitigating the effects of main motor and spin motor plume heating. The main motor has a much longer burn time than the spin motors (~67 s burn time vs. ~0.25 s), however the peak heat rates produced by the spin motors are predicted to be roughly two orders of magnitude larger than those produced by the main motor. Although the main motor plume heating contributes a majority of the integrated heat load, the severe heat rates predicted for the spin motor plume necessitate the use of additional thermal protection in localized areas to protect against burn through.

The spin motors are located on the exterior of the test vehicle and are shown in Figure 4 with and without the thermal protection system (TPS). The spin motor nozzle exit cone is painted white to reduce the effect of direct incident sunlight on the spin motor temperature. The spin motors are mounted to the top deck using titanium brackets and inserts. The low thermal conductivity of the titanium brackets protects the top deck from spin motor soak back heating. The spin motor TPS primarily consists of a low density fibrous alumina insulation encapsulated in a high temperature glass fabric. The insulation keeps the motors from getting too cold during the cold ascent through the troposphere and prevents the spin down motors from getting too hot during the main motor burn. Compression of the low density fibrous insulation is considered acceptable as long as a certain thickness of insulation is maintained. Previous studies have reported that the thermal conductivity of low density fibrous insulation actually decreases when the insulation is compressed by up to 50% [12]. This is likely because higher density fibrous insulators have more barriers to internal thermal radiation and convection per volume than lower density fibrous insulators, resulting in a lower measured thermal conductivity of the material. In certain regions, spin motor plume shields are used to protect the top deck, parachute bridle, and parachute rigging TPS from the severe spin motor plume heating. The steel plume shields are bonded to the top deck using titanium stand-offs with high temperature ceramic washers to thermally isolate the shields from the top deck. The shields are painted with high temperature white paint to keep the initial temperature of the plume shields low prior to spin motor and main motor ignition. In addition to the plume shields, a brush on silicone ablator provided by Ames Research Center is used on selected top deck locations to prevent burn through of the encapsulated fibrous insulation during spin motor plume heating.

The thermal design of the spin motor sub-system for the LDSO test vehicle shares some similarities with the BLDT test vehicle. The spin motors for the BLDT test vehicle also were insulated and mounted on the exterior of

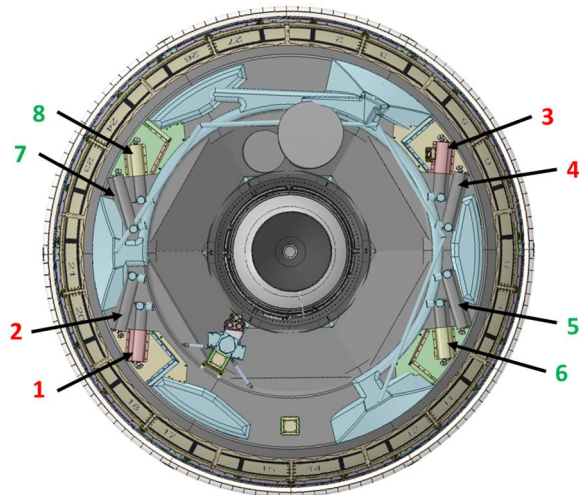


Figure 3. Spin motor numbering on the test vehicle. Spin up motors (1-4) are denoted by red text and spin down motors (5-8) are denoted by green text.

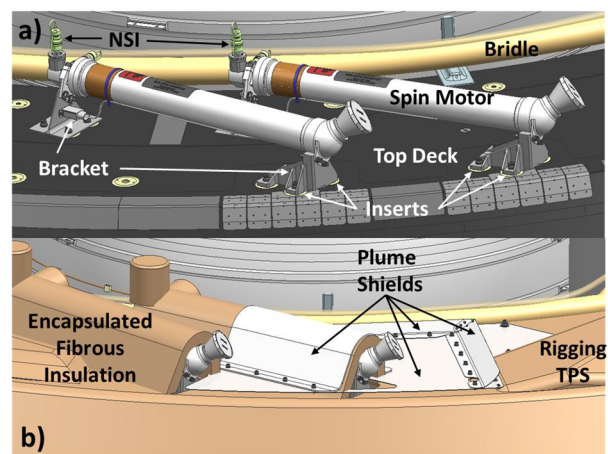


Figure 4. Spin motor sub-system: a) without TPS b) with TPS.

the test vehicle. They were insulated with one inch thick low-density fiberglass encapsulated in antistatic Dacron fabric [10]. However, on the BLDT test vehicle, the spin motor plume heating was determined by analysis to be negligible. This is likely because the exterior portions of the BLDT test vehicle structure were largely made of metal, whereas the LDS test vehicle structure is made of a composite with a narrow allowable temperature range, which is summarized in Table 1. Metals have a higher thermal inertia than structural composites or insulators and can better absorb high heat fluxes for a short duration of time. The metallic spin motor plume shields are necessary to mitigate the substantial risk of encapsulated fibrous insulation burn through during the spin motor burn.

III. Spin Motor Sub-System Requirements

The spin motor sub-system was subject to a number of temperature requirements, summarized in Table 1. The allowable flight temperatures (AFTs) are the temperature limits which the hardware is allowed to reach in flight, and the qualification temperatures are the temperature limits to which the hardware was tested [13]. *The hardware may be capable of more extreme temperatures, but its performance may not be verified.* The requirements are further split up into operational and nonoperational regimes. For example, the spin motors are allowed to experience a wider range of temperatures during nonoperation than they they can immediately before triggering the firing sequence. After that, their temperature will rise rapidly due to internal heat generation and the AFTs no longer apply. The top deck should remain below its operational AFT for the duration of the flight up until the end of testing, when peak structural loads are experienced during parachute snatch. After that, during the nonoperational regime, the vehicle will slowly descend to the ocean’s surface and have plenty of structural margin.

Table 1: Summary of allowable flight temperatures (AFTs) and qualification temperatures.

Component	Allowable Flight Temperature (°C)				Qualification Temperature (°C)			
	Operational		Nonoperational		Operational		Nonoperational	
	Min	Max	Min	Max	Min	Max	Min	Max
Spin Motor	-39	54	-39	54	-54	74	-54	74
Top Deck	-43	64	-43	88	-58	84	-58	108
Fibrous Insulation	-45	730	-45	730	-60	750	-60	750
Insulation Encapsulant	-45	730	-45	730	-60	750	-60	750

The temperature limits on the fibrous insulation and encapsulant were established through high temperature oven testing. Two types of oven testing were performed. In the first, a steel block was placed in a high temperature oven and its temperature allowed to equilibrate. The block was then removed and placed onto a room temperature sample, where a thermocouple measured the contact temperature between the block and the sample. In the second test, the entire sample was placed inside the high temperature oven. Both the fibrous insulation and encapsulant were successfully tested up to 750 °C without any signs of melting or burning.

An additional requirement also states that the temperature difference between the two spin motors in a spin motor pair shall be 8 °C or less when the spin motors are fired. Because the amount of force produced by the spin motor is slightly dependent on the initial propellant temperature, this requirement exists in order to ensure that a mismatched force generated by a pair of spin motors will not change the vehicle trajectory or cause excessive vehicle nutation. Each spin motor temperature will be monitored during ascent using a thermocouple and the data will be used to inform the real time decision to initiate the test sequence for the vehicle.

IV. Spin Motor Thermal Model Calibration

When a spin motor fires, it generates a significant amount of heat and the motor casing and nozzle exit cone get very hot. The implementation on the LDS test vehicle only exacerbates the problem. The spin motors are insulated as much as possible to protect them from main motor plume heating, but this insulation prevents the spin motors from rejecting heat after they fire. This is a concern for the top deck, where the spin motors are mounted. During spin motor ground testing, thermocouples were added to different parts of a spin motor to quantify the amount of energy released during spin motor fire. Testing was performed at atmospheric pressure. The spin motors were chilled in a temperature controlled chamber and removed just prior to testing in order to match the predicted flight firing temperatures as closely as possible. Figure 5 shows the test setup and spin motor components before and during the firing test along with a thermal model of the test setup.

A thermal model of the spin motor test setup was constructed in the thermal analysis tool Thermal Desktop®. The model considered the conductive heat flow from the spin motor to the test stand, and contained boundary conditions to represent natural convection and radiation to the environment. The initial condition of the spin motor was set to the chamber temperature, and the initial condition of the test stand was set to the ambient air temperature. The analysis began when the spin motor was removed from the temperature chamber and ended after the spin motor was fired. A total of five time-varying heat loads to different segments of the spin motor were created and calibrated so that the modeled temperature response matched the test firing data as closely as possible. The temperature response of six discrete points on the thermal model match the test data well and are shown for comparison in Figure 6.

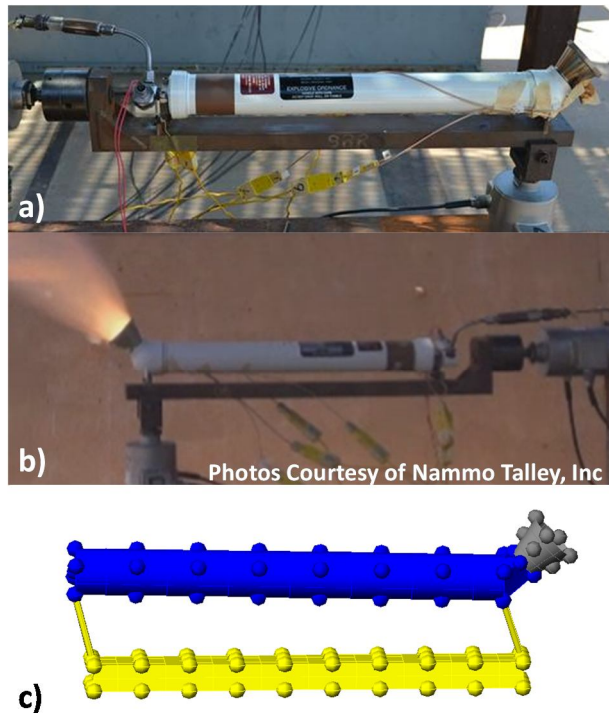


Figure 5. Spin motor test setup: a) before firing b) during firing c) thermal model.

The analysis began when the spin motor was removed from the temperature chamber and ended after the spin motor was fired. A total of five time-varying heat loads to different segments of the spin motor were created and calibrated so that the modeled temperature response matched the test firing data as closely as possible. The temperature response of six discrete points on the thermal model match the test data well and are shown for comparison in Figure 6.

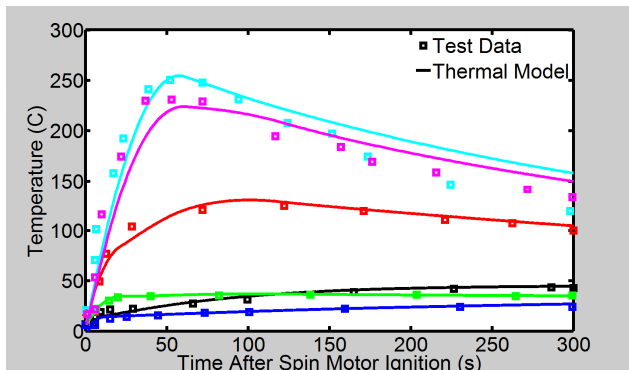


Figure 6. Temperature response of six discrete locations on the thermal model in comparison to the test data.

V. Spin Motor Plume Heating Predictions

The spin motor solid rocket plumes are by nature two-phase; consisting of gaseous hot combustion products and solid aluminum-oxide particles, as they have agglomerated, shattered, and solidified once exiting the nozzle [14]. Spin motor plume heating is caused by three different mechanisms: heat transfer from plume particle thermal energy, plume particle kinetic energy, and gaseous convection. Plume induced environments were predicted at discrete times during the spin motor and main motor firing events. The main motor plume heating environment is beyond the scope of this paper. The trajectory and freestream conditions used for the analysis correspond to the expected flight trajectory with the spin up and spin down respectively occurring at approximately 120,000 and 164,000 ft (36 and 50 km) altitude (Figure 2).

Engineering codes and computational fluid dynamics (CFD) were used to predict the plume induced environments. The Plume Impingement (PLIMP) engineering code was used to predict the particle thermal and kinetic heating on the test vehicle [15-16]. Chamber conditions, provided by the spin motor contractor (NammoTalley, Inc) were used to generate gas thermodynamic properties using the Chemical Equilibrium Combustion (CEC) program [17-18]. The CEC code computed the chemistry and thermodynamic transport properties from the chamber throughout the expansion process to the nozzle exit plane. The combustion chamber/nozzle solution for the spin motor nozzle was performed using the Reacting and Multiphase Program, version 2 (RAMP2) [19-20]. The RAMP2 program is a single or multi-phase inviscid method of characteristics supersonic flow code that fully couples the momentum and heat transfer processes that occur in solid rocket motors between the gas and condensed alumina particulates. The CEC and RAMP2 codes are heritage, computationally efficient, codes that have been developed and utilized over the last 30 years. The nozzle boundary layer properties were generated using the Boundary Layer Integral Matrix Procedure code [21]. At a certain point in the flow, the obtained nozzle flow field solution was extracted and post-processed to be used as a prescribed boundary condition in the CFD grid, which consisted of around 173 million cells. The plume impingement flow field was modeled using

the CFD code, Loci-CHEM 3.2 [22-26]. The CFD flow field model characteristics and assumptions are summarized in Table 2, and the surface mesh and prescribed nozzle inlet boundary are shown in Figure 7.

Table 2: CFD setup and flow model characteristics.

Boundary Conditions	No-slip, isothermal walls
Chemical Species	Frozen 2 species: equivalent air and equivalent plume gas
Compressibility Correction	Sarkar
Diffusion Model	Laminar-Schmidt
Discretization	2 nd order time and space
Thermodynamic Properties	Thermally perfect, temperature dependent specific heat
Turbulence Model	Shear Stress Transport, SST
Viscosity Model	Sutherland

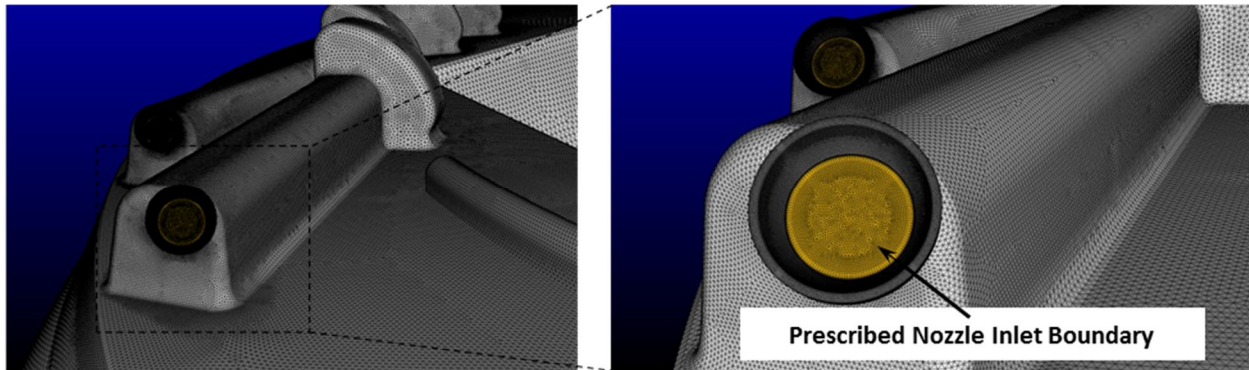


Figure 7. Spin up motor surface mesh with prescribed nozzle inlet boundary.

The predicted spin motor plume flow field mach contours are shown for spin up and spin down in Figure 8, a and b, respectively. The spin up plume is smaller and more concentrated than the expanded spin down plume due to the altitude difference of both simulations. The nozzle flow is highly under expanded for both altitudes and the plume expansion at the nozzle exit affects the local plume impingement heating and impacted area. This means that at spin up, the plume is smaller but heating is more severe, and at spin down the plume heats more area at a generally less severe heat rate. The representative plume heating on a set of spin motors is shown in Figure 8c. The region of highest heating is on the adjacent spin motor case, however other areas experience significant spin motor plume heating as well. The predicted heat rates are on the order of 100 W/cm² or greater.

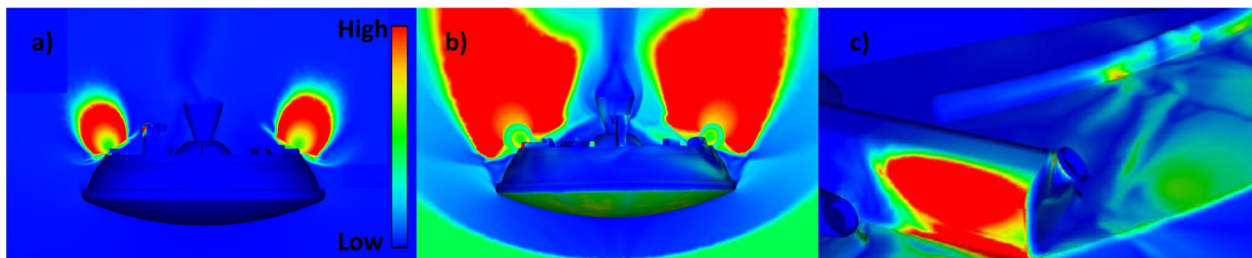


Figure 8. Selected CFD simulation results: a) mach contour for the spin up plumes b) mach contour for the spin down motor plumes c) heat flux contour on the spin motor case, bridle, and top deck.

VI. Plume Shield Temperature Predictions

With extremely high heat rates, a very low thermal inertia material such as fibrous insulation rapidly approaches radiative thermal equilibrium. This can be verified using the analytical solution for the surface temperature of a semi-infinite body subjected to a constant heat flux [27], shown in Equation 1.

$$T_s(t) = T_i + 2q'' \sqrt{\frac{t}{\pi k \rho c_p}} \quad (1)$$

In this equation, T_i is the initial temperature of the semi-infinite body representing the insulation, q'' is the surface heat flux, t is time, π is Pi, k is thermal conductivity, ρ is density, and c_p is specific heat. Equation 1 only holds true for a short time because as the insulation surface temperature rises, so does the thermal radiation emitted from the surface. As a result, a simple energy balance can be used to estimate the peak surface temperature, shown in Equation 2.

$$T = (q''/\sigma\varepsilon)^{0.25} \quad (2)$$

In this Equation, T is temperature, q'' is heat flux, σ is the Stefan-Boltzman constant, and ε is the thermal emissivity. With a heat flux on the order of 100 W/cm² or greater, the surface temperature can exceed 1500 °C during the 0.25 s spin motor firing, even though the fibrous insulation and encapsulant were only qualified to 750 °C. As a result, low thermal inertia fibrous insulation alone is not sufficient to protect against the spin motor plumes due to the serious risk of burn through. Instead, metallic plume shields are sized and designed to protect the vehicle in peak heat flux regions. AISI 304 steel is chosen as the shield material due to its high melting point, low cost, relatively high thermal conductivity, and the availability of well documented temperature dependent material properties [27, 28].

A 1D numerical model was used to predict the through thickness steel temperature of the plume shields. The model considered the worst case combination of heat loads from the spin motor and main motor plumes, and used an adiabatic boundary condition for the shield backside. The heated surface was radiatively coupled to a node representing the environment for the duration of the simulation. At the most severe heating location on the adjacent spin motor, the rocket plume was assumed to erode the paint so that the bare steel was present and the thermal emissivity of the surface was reduced. At other locations, the high temperature paint remained below its allowable temperature. The risk of charring or blackening of the paint could have raised the solar absorptivity after motor fire, but is not expected to change the thermal emissivity. Although the numerical model uses temperature dependent properties and considers surface radiation, and the analytical solution of Equation 1 uses constant material properties and neglects surface radiation, the predicted surface temperature is similar. In this way, the analytical solution is used to validate the numerical model. The numerically predicted surface and backside temperatures at the most severe heating location is plotted vs. time in Figure 9 along with the analytically predicted surface temperature.

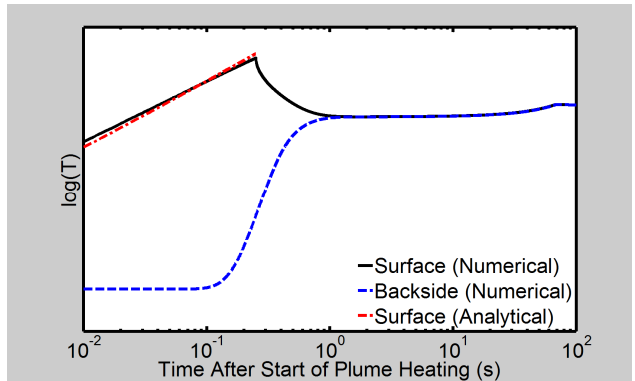


Figure 9. Predicted plume shield temperatures using numerical and analytical methods.

VII. Spin Motor Temperature Predictions

In order to obtain temperature predictions for the spin motors during flight, it was necessary to integrate the calibrated spin motor model into the LDS system level thermal model, which was described in detail in a previous paper [11]. First, the spin motors were conductively coupled to the top deck of the test vehicle. The nodal discretization of the top deck had to be refined in order to properly capture heat spreading from the spin motor bracket to the top deck composite. The mass of the spin motor brackets and top deck inserts were represented using a single node for each bracket and a single node for each group of inserts. The conductance values were obtained through a resistance network analysis which used tabulated bolted joint resistances and conductance values obtained through a finite element analysis of the spin motor brackets and top deck inserts. TPS was added to the model around the spin motors, and time-varying heat loads were applied to the TPS to represent the main motor and spin motor plume heating. Uncertainties in the environment and convection coefficients were accounted for through the use of worst case hot (WCH) and worst case cold (WCC) bounding environments. The same bounding thermal environments and convection coefficients, previously described in detail [11], were used in this work. Both radiation and air convection were considered on the exposed surfaces of the spin motors and TPS. Two spin motors in the completed thermal model are shown in Figure 10.

One of the unique thermal challenges for the spin motor sub-system is taking into account the changing and uncertain thermal environments around the test vehicle, shown in Figure 11. These environments are especially relevant in predicting whether the 8 °C temperature difference requirement for the spin motor pairs is met. Although largely symmetrical, the entire vehicle hangs from a balloon at a 24 degree nominal hang angle. In reality, the hang angle could be anywhere from 17 to 30 degrees. The hang angle can affect the albedo, sky IR, ground IR, and direct solar flux on both sides of the test vehicle and the spin motors. In addition, the vehicle naturally spins at a rate of approximately 1 RPM as it ascends to its float altitude. This is good because it spreads the direct solar flux evenly around the vehicle through the ascent. However, once the vehicle reaches float altitude, it may or may not continue to spin. If it does not spin, the natural pointing direction of the vehicle would be random. The balloon has the ability to spin or point the vehicle prior to initiation of the motor firing sequence, but it is desirable that the vehicle has a robust design regardless of pointing. For the WCH orbit, the sun passes directly overhead the vehicle at noon, but in a WCC orbit, the sun reaches a maximum elevation angle of 65 degrees from the horizon. The WCH environment also has a much larger albedo than the WCC environment (0.35 vs. 0.06) [11].

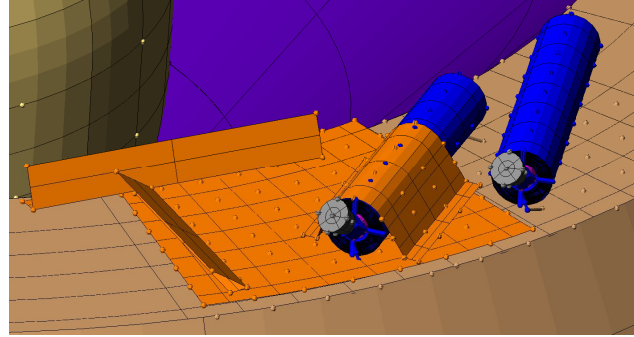


Figure 10. The spin motor thermal model was integrated into the LDS system thermal model along with the spin motor TPS.

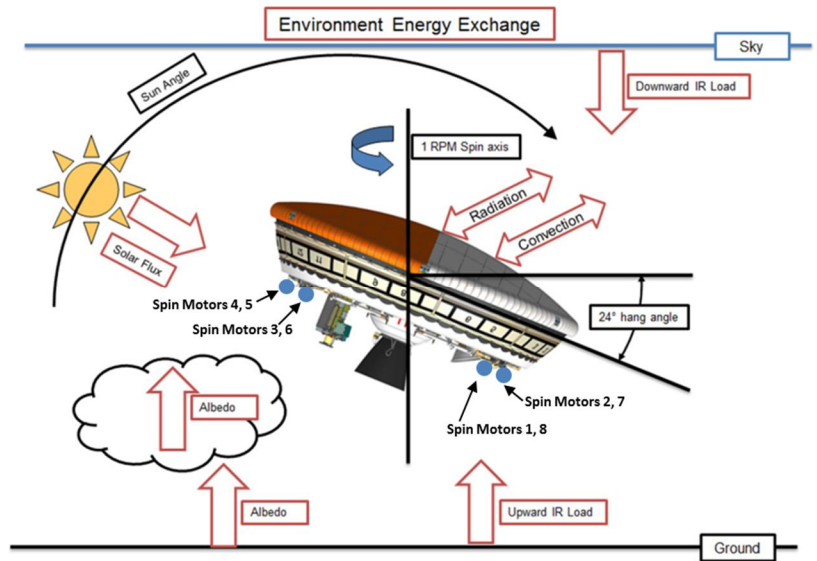


Figure 11. The vehicle thermal environments and their relation to the spin motors [11].

Due to the uncertainty in the environment for the test vehicle and the influence that this may have on individual spin motor temperatures, a rigorous set of analyses were performed to better understand the effect of hang angle, vehicle spin, pointing direction, and sun angle on the spin motor temperatures. The temperature of the spin motors vs. time after start of ground operations for both WCC and WCH in the nominal condition (fast spin, 24 degree hang angle) and the conditions which represent the largest predicted temperature difference for both WCC and WCH are shown in Figure 12. The worst predicted temperature difference in a spin motor pair is 5 °C for WCH (Figure 12, c) and 7 °C for WCC (Figure 12, d).

Numerous trends were observed, some more obvious than others. First, a spinning vehicle is preferable to a non-spinning vehicle because the spinning spreads the solar loads more evenly on the various spin motors. Second, a larger hang angle corresponds to larger temperature differences between spin motor pairs. This is because the spin motors in a single pair are on opposite sides of the vehicle (Figure 3) with spin motors 4 and 5 having a better view of the sky, and spin motors 2 and 7 having a better view to the ground and albedo (Figure 11). The consequence of this point is that spin motors 4 and 5 tend to be colder than spin motors 2 and 7, unless spin motors 4 and 5 receive direct sunlight. Spin motors 1, 3, 6, and 8 tend to have more uniform temperatures because they are on the interior of the vehicle and are “shaded” from the extremes that spin motors 2, 4, 5, and 7 experience. Third, the interior spin motors (2, 4, 5 and 7) are predicted to be slightly colder on average than the other spin motors because they are partially covered by the plume shields. The plume shields are painted white and have a lower solar absorptivity than the fibrous insulation encapsulant. All these trends are evident in Figure 12, a-d.

Other trends were less obvious. These are best explained by close examination of Figure 12, c and d. It is interesting that for WCH, the worst direction for the vehicle aeroshell to point is to the SE (Figure 12, c), while for WCC, the worst direction for the vehicle aeroshell to point is to the NW (Figure 12, d). When the vehicle aeroshell

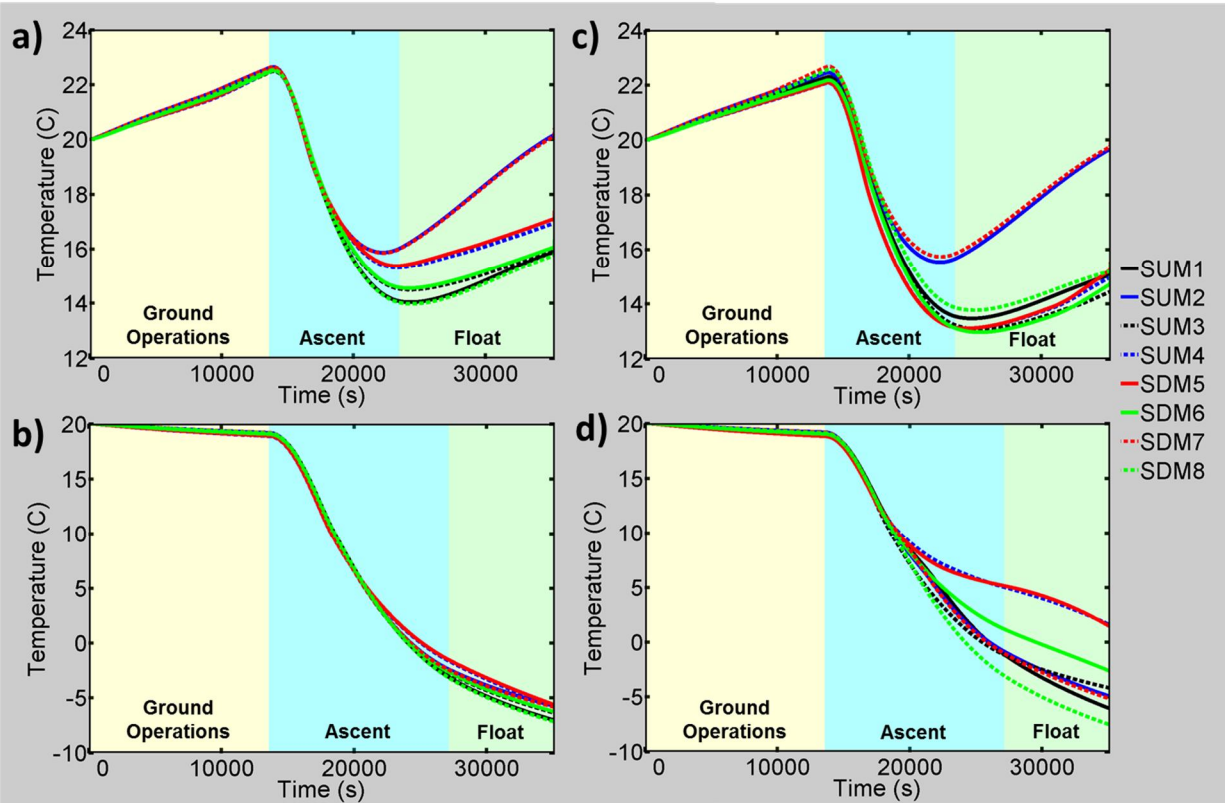


Figure 12. Spin motor temperature predictions: a) WCH environment with a 24 degree hang angle and a fast spin b) WCC environment with a 24 degree hang angle and a fast spin c) WCH environment with 30 degree hang angle and no spin, aeroshell pointing SE d) WCC environment with a 30 degree hang angle and no spin, aeroshell pointing NW.

points to the SE in WCH, the albedo is high and the spin motors are totally shielded from direct sunlight. As a result, spin motors 2 and 7 are much warmer than spin motors 4 and 5. When the vehicle aeroshell points to the NW in WCC, spin motors 2 and 7 receive very little albedo and spin motors 4 and 5 receive a significant amount of direct sunlight. As a result, spin motors 4 and 5 get significantly warmer than motors 2 and 7. The only reason this is possible in WCC is because the sun is at the lowest elevation angle possible within the launch window. For the WCH environment with no vehicle spin and the aeroshell pointed to the NW (not shown), the sun angle is higher and the heating of spin motors 4 and 5 by direct sunlight is partially blocked by the aeroshell.

Ultimately, the spin motor sub-system is predicted to meet the 8 °C temperature difference requirement for the spin motor pairs, but without much margin. On flight day, the spin motor temperatures can be monitored and some adjustments could be made if necessary. If the vehicle is not spinning freely, then it is possible that it could be intermittently rotated “rotisserie” style, using the vehicle’s rotator mechanism. Alternatively, if spin motors 4 and 5 need to be heated up relative to motors 2 and 7, the test vehicle can be pointed with the aeroshell to the NW so that sunlight heats up motors 4 and 5. In the opposite case where spin motors 4 and 5 need to be cooled down relative to motors 2 and 7, the vehicle can be pointed with the aeroshell to the SE to block the sunlight that may heat up motors 4 and 5.

VIII. Top Deck Temperature Predictions

The final major thermal concern centered around keeping the top deck below its AFTs after spin motor firing. The top deck AFT is set at 64 °C operational, 88 °C nonoperational on the hot side in order to maintain the structural integrity of the test vehicle. Operational is defined as before the end of the parachute test period, when the loads are high, and nonoperational is defined as after the test period, during descent, when the structural loads are low. The spin motors presented numerous threats to the top deck. After the spin motors fire, they are expected to significantly increase in temperature due to internal heat generation, as discussed previously in Section IV. However, the spin

motors are conductively coupled with the top deck through the spin motor brackets. As a result, the brackets were made from a titanium alloy with a low thermal conductivity. The predicted temperature of the brackets and top deck is shown in Figure 13. Although the predicted temperatures are very close to the AFTs, there is a 20 °C margin between the hot side AFT and qualification temperature, which is standard practice at JPL [13].

A separate detailed model was made to consider localized heating of the top deck underneath the titanium stand-offs which support the plume shields. The worst case heating environment for top deck heating is the spin up plume heating followed by main motor heating. This is because the spin up plume heating is more severe than the spin down plume heating since the spin up takes place at a higher atmospheric pressure than spin down, confining the rocket plume and increasing the heat rate. In addition, the spin up plumes heat up the plume shields at the earliest possible moment so that the heat has more time to propagate to the top deck. High temperature ceramic washers and low thermal conductivity titanium stand-offs are used to thermally isolate the spin motor plume shields from the top deck. The maximum temperature of the top deck occurs directly underneath the titanium stand-offs. The maximum predicted top deck temperature is illustrated in Figure 14.

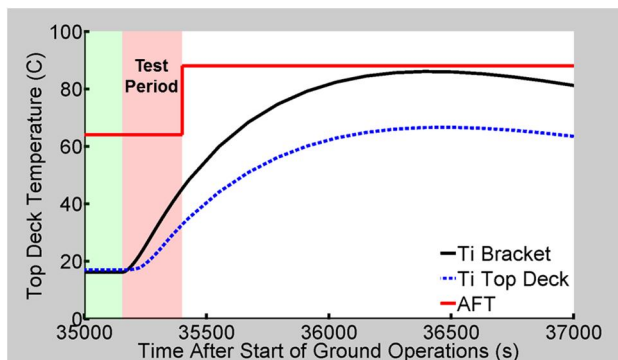


Figure 13. The WCH predicted temperature of the top deck and spin motor brackets.

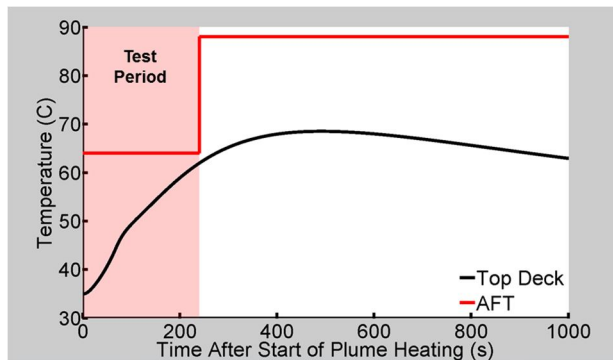


Figure 14. The WCH predicted temperature of the top deck underneath the titanium stand-offs.

IX. Conclusion

The spin motor sub-system is predicted to meet all of its requirements with margin, using only passive thermal control. A careful and rigorous analysis shows that the spin motors are predicted to stay well within their AFT limits, and that spin motors in a single pair will be within 8 °C of each other prior to spin motor fire. This will help ensure the correct vehicle trajectory. The top deck also will stay within its operational and nonoperational AFT limits using titanium alloy spin motor brackets and thermal isolation of the spin motor plume shields. Keeping the top deck within its AFT is necessary to maintain the structural integrity of the test vehicle during parachute deployment. Finally, the TPS consisting of high temperature insulation and steel plume shields is predicted to remain within its capabilities during both the ultra-high heat flux loads from the spin motor plume heating, as well as the longer but less intense main motor plume heating.

Acknowledgments

The development described in this paper was carried out at the Jet Propulsion Laboratory, California Institute of Technology, under a contract with the National Aeronautics and Space Administration. The authors express their thanks to NASA's Office of the Chief Technologist for supporting this effort and enabling a select few to push the envelope. The authors wish to thank several of their colleagues who have been instrumental to the thermal task at hand: Jason Kempenaar, Brenda Hernandez, Sandria Grey, Brant Cook, Kevin Burke, John-Luke Wolff, Eric Oakes, Mark Duran, Richard Frisby, Gabriel Molina, Christopher Porter, Guillermo Blando, Carl Guernsey, Mark Yerdon, and Morgan Parker. The authors also wish to thank Bud Smith (MSFC) for heat transfer from the plume particle thermal and kinetic energies, Robin Beck and Deepak Bose (ARC) for valuable advice, and Nammo Talley, Inc for supplying test firing data and images. Reference herein to any specific commercial product, process, or service by trade name, trademark, manufacturer, or otherwise, does not constitute or imply its endorsement by the United States Government or the Jet Propulsion Laboratory, California Institute of Technology.

References

- ¹Lundstrom, R.R., Raper, J.L., Bendura, R.J., and Shields, E.W., "Flight Tests of Viking Parachute System in Three Mach Number Regimes I: Vehicle Description, Test Operations, and Performance," NASA Technical Note TN D-7692, 1974.
- ²Bendura, R.J., Lundstrom, R.R., Renfroe, P.G., and LeCroy, S.R., "Flight Tests of Viking Parachute System in Three Mach Number Regimes II - Parachute Test Results," NASA Technical Note TN D-7734, pp. 1-96, 1974.
- ³Raper, J.L., Michel, F.C., and Lundstrom, R.R., "The Viking Parachute Qualification Test Technique," in AIAA 4th Aerodynamic Deceleration Systems Conference, Palm Springs, CA, 1973.
- ⁴Smith, B.P., Tanner, C.L., Mahzari, M., Clark, I.G., Braun, R.D., and Cheatwood, F.M., "A Historical Review of Inflatable Aerodynamic Decelerator Technology Development," in IEEE Aerospace Conference, Big Sky, MT, 2010.
- ⁵Gallon, J.C., Clark, I.G., Rivellini, T.P., Adams, D.S., and Witkowski, A., "Low Density Supersonic Decelerator Parachute Decelerator System," in AIAA Aerodynamic Decelerator Systems Conference, Daytona Beach, FL, 2013.
- ⁶Giersch, L., Rivellini, T., Clark, I., Shook, L., Ware, J., and Welch, J., "SIAD-R: A Supersonic Inflatable Aerodynamic Decelerator for Robotic Missions to Mars," in AIAA Decelerator Systems Conference, Daytona Beach, FL, 2013.
- ⁷Coatta, D., Jurewicz, D., Tutt, B., Rivellini, T., Clark, I., "Development and Testing of an 8 Meter Isotenoid Supersonic Inflatable Aerodynamic Decelerator," in AIAA Aerodynamic Decelerator Systems Conference, Daytona Beach, FL, 2013.
- ⁸NASA, "Fact Sheet: Low Density Supersonic Decelerators," 26 March 2013. [Online]. Available: http://www.nasa.gov/pdf/737628main_Final_LDSD_Fact_Sheet_3-26-13.pdf. [Accessed 20 January 2014].
- ⁹Cook, B.T., Blando, G., Kennett, A., Heydt, M.V., Wolff, J.L., and Yerdon, M., "High Altitude Supersonic Decelerator Test Vehicle," in AIAA Aerodynamic Decelerator Systems Conference, Daytona Beach, FL, 2013.
- ¹⁰Buna, T., and Battley, H.H., "Thermal Design and Performance of the Viking Balloon Launched Decelerator Test Vehicles," in AIAA/ASME Thermophysics and Heat Transfer Conference, Boston, MA, 1974.
- ¹¹A. J. Mastropietro, M. Pauken, E. Sunada and S. Gray, "Thermal Design and Analysis of the Supersonic Flight Dynamics Test Vehicle for the Low Density Supersonic Decelerator Project," in International Conference on Environmental Systems, Vail, CO, 2013.
- ¹²Graves, R.S., and Yarbrough, D.W., "The Effect of Compression on the Material R-Value of Fiberglass Batt Insulation," *Journal of Building Physics*, 15, 1992.
- ¹³Gilmore, G. (ed.), "Spacecraft Thermal Control Handbook," 2nd ed., The Aerospace Corporation, 2002.
- ¹⁴Smith, S.D., "Development of a Nozzle/Plume and Plume Impingement Code." CI FR 0089, Continuum, Inc., Huntsville, AL, November 1986.
- ¹⁵Smith, S., "Model Development for Exhaust Plume Effects on Launch Stand Design-PLIMP/LSD," SECA Report SECA-93-FR-9, SECA, Inc., June 1993.
- ¹⁶Salita, M., "Survey of Recent Al₂O₃ Droplet Size Data in Solid Rocket Chambers, Nozzles, and Plumes," 31st JANNAF Combustion Subcommittee Meeting, CPIA Publication 620, Volume 1, October 1994.
- ¹⁷Svehla, R.A., and B.J. McBride, "FORTRAN IV Computer Program for Calculation of Thermodynamics and Transport Properties of Complex Chemical Systems," NASA TN D-7056, January 1976.
- ¹⁸Sulyma, P.R., and L.R. Baker, Jr., "User's Guide for TRAN72 Computer Code Modified for Use with RAMP and VOFMOC Flowfield Codes," LMSC HREC TM D390409, Lockheed Missiles & Space Company, Huntsville, Ala., October 1974.
- ¹⁹Smith, S.D., "High Altitude Supersonic Flow of Chemically Reacting Gas-Particle Mixtures - Volume I - A Theoretical Analysis and Development of the Numerical Solution," LMSC-HREC TR D867400-I, Lockheed Missiles & Space Company, Huntsville, Ala., October 1984.
- ²⁰Smith, S.D., "Update to the RAMP2 Computer Program", SECA-FR-93-19, SECA Inc., Huntsville, AL., December 1993.
- ²¹Evans, R.M., "Boundary Layer Integral Matrix Procedure BLIMPJ User's Manual," UN-75-64 Aerotherm, Mountain View CA., July 1975.
- ²²Luke, E., and George, T., "Loc: A Rule-Based Framework for Parallel Multidisciplinary Simulation Synthesis," *Journal of Functional Programming, Special Issue on Functional Approaches to High-Performance Parallel Programming*, Volume 15, Issue 03, Cambridge University Press, 2005, pp 477-502.
- ²³Luke, E., "A Rule-Based Specification System for Computational Fluid Dynamics," Ph.D. Dissertation, Mississippi State University, December 1999.
- ²⁴Wu, J., Tang, L., and Luke, E., "A Low Mach Number Preconditioning Scheme of the Reactive Roe Flux," 41st AIAA Aerospace Sciences Meeting and Exhibit, January 6-9, 2003, Reno, NV, AIAA #2003-0307.
- ²⁵Luke, E., Tong, X-L., Wu, J., Tang, L., and Cinnella, P., "A Step Towards 'Shape Shifting' Algorithms: Reacting Flow Simulations Using Generalized Grids," 39th AIAA Aerospace Sciences Meeting and Exhibit, January 8-11, 2001, Reno, NV, AIAA Paper #2001-0897.
- ²⁶Liu, Q., Luke, E., and Cinnella, P., "Coupling Heat Transfer and Fluid Flow Solvers for Multi-Disciplinary Simulations," *AIAA Journal of Thermophysics and Heat Transfer*, Volume 19, No. 4, Oct.-Dec. 2005, pp417-427.
- ²⁷Incropera, F.P., and DeWitt, D.P., "Introduction to Heat Transfer," 3rd ed., John Wiley & Sons, 1996.
- ²⁸MIL-HDBK-5, "Military Handbook of Metallic Materials and Elements for Aerospace Vehicle Structures, Defense Area Printing Service, 1998.